Gray Level Image Encoding in Plasmonic Metasurfaces

Ting Zhang 1,2 · Steve Blair 2

Received: 16 October 2019 / Accepted: 11 March 2020 © Springer Science+Business Media, LLC, part of Springer Nature 2020

Abstract

Plasmonic metasurfaces have been widely used for image and color representation using nanoscale structures. By designing the size or shape of nanostructures, the phase or amplitude of transmitted or reflected electromagnetic spectrum can be manipulated via control of resonant wavelength, which results in multiple colors and can be used for color and/or image generation. Instead of color printing, we introduce a new approach from which images with multiple gray scales can be generated and hidden under light with specific wavelengths. In this work, plasmonic structures of nanorods with identical geometries are fabricated in arrays on a glass substrate, but the nanorods comprise binary alloys of aluminum and titanium; therefore, grayscale image information is encoded with the material composition. Under white light illumination with polarization along the long axis of a nanorod, the response of the nanorods has essentially the same resonant frequency, but with varying magnitudes of transmission. Based on this, using nanorods with four different compositions, four gray level imaging has been achieved. Since nanorods are sensitive to the polarization and spectral composition of the incident light, under unpolarized white light illumination, the image disappears. Therefore, this technique is promising in image encryption. We also show that the manipulation of light at the resonant wavelength by this method occurs in amplitude, not phase.

Keywords Plasmonics · Metasurface · Image-encoding

Plasmonic resonance occurs through the interaction of electromagnetic waves with electron oscillations in metals. Metal nanostructures fabricated with varied shapes, dimensions, orientations, and materials lead to manipulations of the amplitude and phase of electromagnetic waves [1, 2]. Applications for such plasmonic metasurfaces abound in new optical devices, such as flat and ultrathin optical components, waveguides, invisibility cloaks, and holograms [3–12]. In particular, plasmonic metasurfaces have emerged in application to color image generation [13–23]. By tailoring an electromagnetic wave's spectrum using nanostructures with spatially varying sizes or shapes, color images with high resolution and gamut can be generated [15–18]. Furthermore, encryption of images has been demonstrated using dynamic plasmonic

Electronic supplementary material The online version of this article (https://doi.org/10.1007/s11468-020-01151-5) contains supplementary material, which is available to authorized users.

- Steve Blair blair@ece.utah.edu
- Department of Physics and Astronomy, University of Utah, Salt Lake City, UT 84112, USA
- Department of Electrical and Computer Engineering, University of Utah, Salt Lake City, UT 84112, USA

metasurface devices [19–25]. Image hiding and generation have been achieved by switching the refractive indices of surrounding materials using phase change materials or chemical reactions [21–23]. Grayscale images have been encoded in the infrared regime, but hidden under visible illumination, using coupled plasmonic resonances [24], and in the visible regime using polarization modulation [25]. However, most work in image generation and encryption using plasmonic metasurfaces so far have relied on careful design of the sizes and/or geometries of nanostructures for generating/manipulating multiple colors or intensities.

In addition, many of reported metasurfaces are designed for manipulating the phase profile of incident electromagnetic waves. However, completely controlling the properties of light requires both amplitude and phase manipulation. By controlling both independently, holographic images with high quality can be generated, which is promising in image and data storage, beam shaping, super lensing, and so forth. Engineering propagating light with multiple levels of amplitude independently from multiple levels of phase has been achieved by changing the plasmonic nanostructure geometry in a few reports [26, 27]. In these references, antennas were designed at micro scales, for which they can be applied in the terahertz or microwave regimes.



We develop a new approach for plasmonic metasurfaces for image generation using an identical geometry for each unit cell in the surface. Instead of generating colors that correspond to different resonant wavelengths within a broadband spectrum, images are created in gray scales that correspond to multiple intensity levels, but only within a specified narrow band of wavelengths. Light amplitude is independently manipulated without phase change by using binary alloys of aluminum (Al) and titanium (Ti) with varying composition fractions across the surface. The encoded image can be observed with high contrast under light with a specific narrow spectral band and polarization direction and is hidden under white light. It is important to highlight that this work experimentally demonstrates the use of effective material permittivity as a variable parameter in a plasmonic metasurface. This is achieved using spatial patterning of calibrated compositions of co-sputtered films of poor and good plasmonic material constituents. Moreover, our results demonstrate a scalable approach where multiple amplitude modulation levels can be achieved without changing the size or shape of the plasmonic structure.

For the geometry of the plasmonic structure, we chose a nanorod based upon its simple geometry and significant plasmonic response to a polarized electromagnetic wave. For nanorod antennas in the optical regime, the $\lambda/2$ dipole length is affected by the skin depth, which modifies the apparent dimensions of the structures. Instead of using the external wavelength λ , an effective wavelength $\lambda_{\rm eff}$, which is related to the geometry and material properties, has been introduced for antenna design [28]. Based on [28], we designed our nanorods with dimension l=200 nm (length), w=80 nm (width), and h=50 nm (thickness). To avoid coupling between rods, the periodicity was designed as a=360 nm, somewhat at the expense of grayscale contrast. The designed and fabricated metasurfaces are shown as Fig. 1a.

We chose aluminum as the base plasmonic material due to its broadband plasmon resonance and environmental stability owing to its native oxide. [29, 30]. To compare the plasmonic response of other candidate metals, we performed finite difference time domain simulations (Lumerical FDTD Solutions) to obtain transmitted spectra across wavelengths from 500 to 850 nm for nanorod arrays of the same size, but comprised of different materials: Al, gold (Au), silver (Ag), and copper (Cu), all of which have low losses in the visible range. The calculated transmission spectra with these different materials are shown in Fig. 2a. Resonance for the Al nanorod is located around 650 nm, while resonances for the nanorod with the other materials are located around 800 nm. For nanorods with identical geometry, but different material, the resonance for Al is located at a shorter wavelength than with Au, Ag, or Cu, easing fabrication requirements for structures with visible response. [19]

The utilization of Ti in a binary alloy with Al is based on its high loss at visible wavelengths compared with other metals. Figure 2b shows the calculated transmission spectra for the designed nanorod arrays with the same size, but comprised of different high loss materials. Compared with other materials, nanorods of Ti have negligible plasmonic response across the wavelength range 500–850 nm. From this analysis, we conclude that Al and Ti are suitable materials to be combined in controlled fractions for manipulating the plasmonic response at visible wavelengths. Based on this, nanorod arrays with identical geometry but different compositions of Al and Ti were designed to produce spatially varying amplitudes of transmitted light at a specific wavelength.

To verify this presumption, thin films (50 nm thickness) with volume percentages of 100%Al, 97%Al:3%Ti, 94%Al:6%Ti, 90%Al:10%Ti, 85%Al:15%Ti, and 80%Al:20%Ti were separately deposited on glass slides by co-sputtering (Denton Discovery 18). The complex refractive indices n+ik of these six films were measured by a Variable Angle Spectroscopic Ellipsometer (Woollam VASE). The complex permittivity $\varepsilon_r + i\varepsilon_i$ was calculated from n and k for each material, as shown in Fig. S1(a) and S1(b). The ratio $-\frac{\varepsilon_r}{2}$

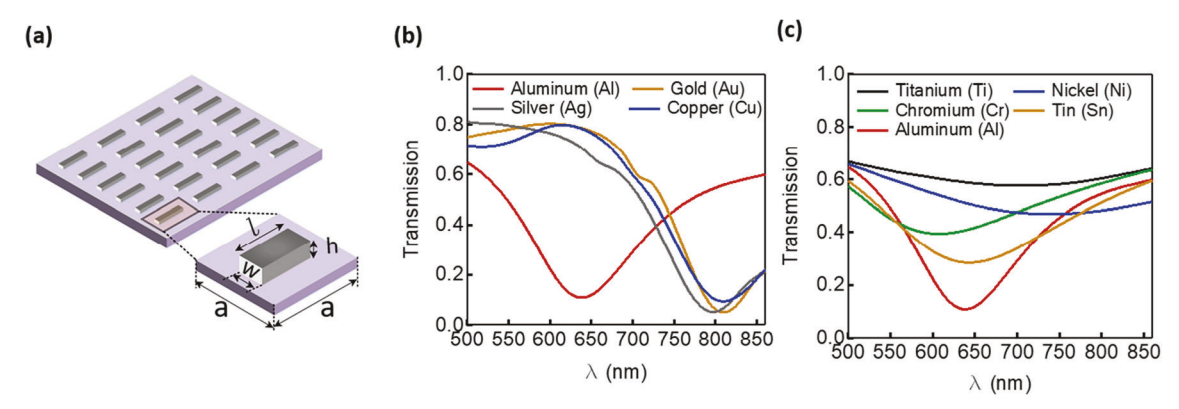


Fig. 1 Calculated transmission spectra based on FDTD simulations for nanorod antenna arrays with 200 nm length, 80 nm width, 50 nm height, and 360 nm periodicity, but with different metals. **a** Schematic drawing of the rectangular array, where the nanorod and unit cell dimensions are l =

200 nm, w = 80 nm, h = 50 nm, and a = 360 nm. Light transmission calculations with plasmonic materials Al, Au, Ag, and Cu. **b** Calculation with the "poor" plasmonic metals Ti, Cr, Fe, Ni, Sn, and W, compared with Al



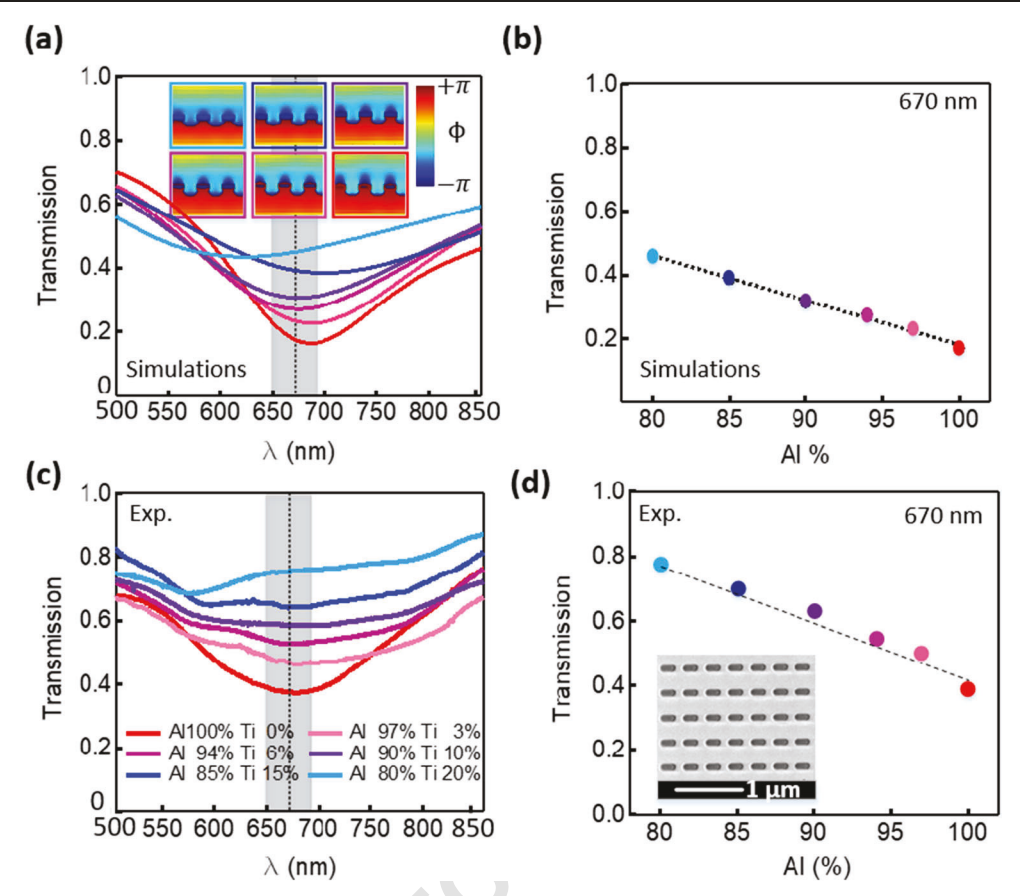


Fig. 2 Characterization of the plasmon resonance of composition-modulated nanorod arrays. **a** Simulated response of the nanorod array with different compositions of co-sputtered films. The simulated phase profile in cross-section of the metasurface, in the inset, for different material compositions shows the metasurface allows for amplitude-only modulation. The dimensions of the nanorods used here are the same as defined in Fig. 1a. **b** Corresponding average values of transmission across the desired wavelength range of 650–690 nm. **c** Measured optical

transmission response of a 10×10 array for each material composition and ${\bf d}$ corresponding average transmission across 650–690 nm. Both simulations and measurements show linear modulation of transmitted amplitude with Al % in the co-sputtered material. The inset in ${\bf d}$ shows scanning electron micrograph of the nanorod metasurface. The metasurface was fabricated using focused ion beam milling. The curves in ${\bf a}$ - ${\bf d}$ and boxes around the phase profile in the inset are color coded as per the legend given in ${\bf c}$

is a common figure of merit relating to the field enhancement due to localized surface plasmon resonance [31]. The calculated values of $-\frac{\varepsilon_r}{\varepsilon_i}$ for all 6 materials at a wavelength of 670 nm are shown in Fig. S1(c) which is plotted as a fraction of Al from 80 to 100%. This plot implies that the alloy has a reduced plasmonic response as the fraction of Ti increases. Both Al and Ti form native oxides as alumina and titania, which are self-limiting layers that passivate the bulk metal.

The measured refractive indices were used in the simulation of the plasmonic response of these nanorods with the different alloy compositions. In the FDTD simulations, nanorods were placed on SiO_2 in a 10×10 array for each composition. The transmission spectra are shown in Fig. 2a. In Fig. 2b, we calculated the average value of transmission across the wavelength range 650 nm to 690 nm for Al fractions from 100 to 80%, which shows that the amplitudes for average transmission are linear with the Al fraction. We note that for simplicity, we did not explicitly model the nanorod in a core-shell (metal-oxide) structure, and instead relied on that fact that

both the reflection measurements in ellipsometry and surface plasmon response are surface sensitive, and assumed that the optical penetration depths in both cases are similar. Thus, the effective permittivity values extracted from ellipsometry would account for the surface properties including native oxide.

We next fabricated 10×10 nanorod arrays on films with different Al:Ti compositions by focused ion beam (FIB). The beam current for FIB lithography is 7.7 pA and is used for removing materials from around the rods. Nanorod arrays were fabricated with length, width, and height of 200 nm, 80 nm, and 50 nm, respectively, and the periodicity of the array is 360 nm. The SEM image for one nanorod array is shown in Fig. 2d. In addition, we milled transparent square windows of size 3.8 μ m \times 3.4 μ m (the same size as the area of the nanorod dipole arrays) for light transmission references. Samples with nanorod arrays were placed on the sample holder of a microscope, with white light passing through a linear polarizer oriented along the long axis of the nanorods. The



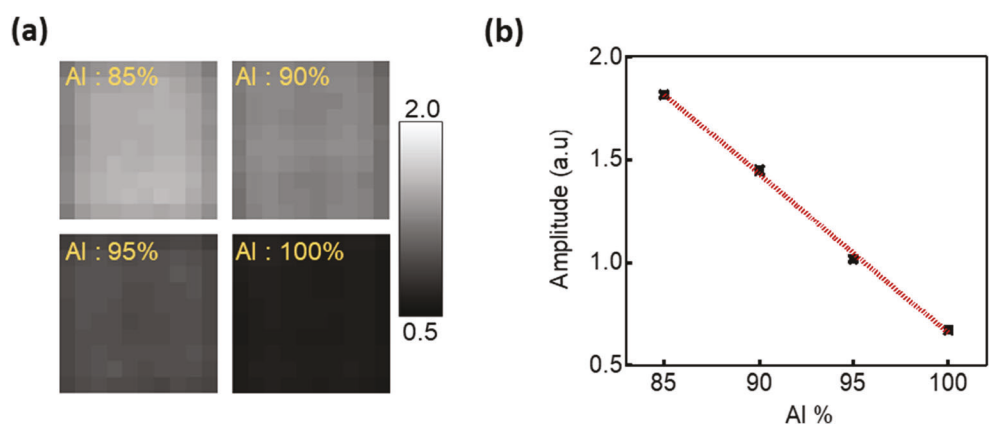


Fig. 3 a Optical transmission images through the metasurface for a 10×10 nanorod antenna array for different compositions of Al:Ti. Incident light is linearly polarized along the nanorod major axis and bandpass filtered (650–690 nm). Images are labeled with % composition of Al. **b**

Average gray-level value light intensity for the 4 sets of Al composition. Again, a linear variation is observed, highlighting the scalability of the approach

transmitted light then goes to a CCD camera or a spectrometer for analysis over a spectral range 500–850 nm. The light passing through the polarizer illuminates the nanorod arrays, or the open windows for reference, and spectral transmittance is obtained by dividing the spectral amplitude transmitted through the nanorod arrays by the spectral amplitude transmitted through the square windows. Figure 2c shows the transmittance spectra for nanorod arrays with the six Al:Ti alloys. The plasmonic resonances are located at or near 675 nm for all samples. We then calculated the average transmittance values

across the 650-690 nm wavelength range. These average values are linear with the fraction of Al, as shown in Fig. 2d.

In general, experimental results are consistent with simulation results. The curves in the spectra for the experimental results are flatter at the bottom compared with the simulation results, which arises from the fact that in the model, we use a perfect rectangle for the nanorod shape, while for the fabricated nanorods, the ends are rounded, and the side walls are not straight, making the area of the top surface smaller than the bottom surface, which reduces the resonance.

Fig. 4 Fabrication process of the composition-encoded grayscale metasurface. Steps, in clockwise order, start from the background (blocking) Ti film on a glass substrate, to subsequent patterning of the letters in "UTAH," each with a different composition of Al:Ti alloy films. At the final stage, nanorod arrays were fabricated using FIB milling within a square boundary enclosing each letter to produce the plasmonic metasurface

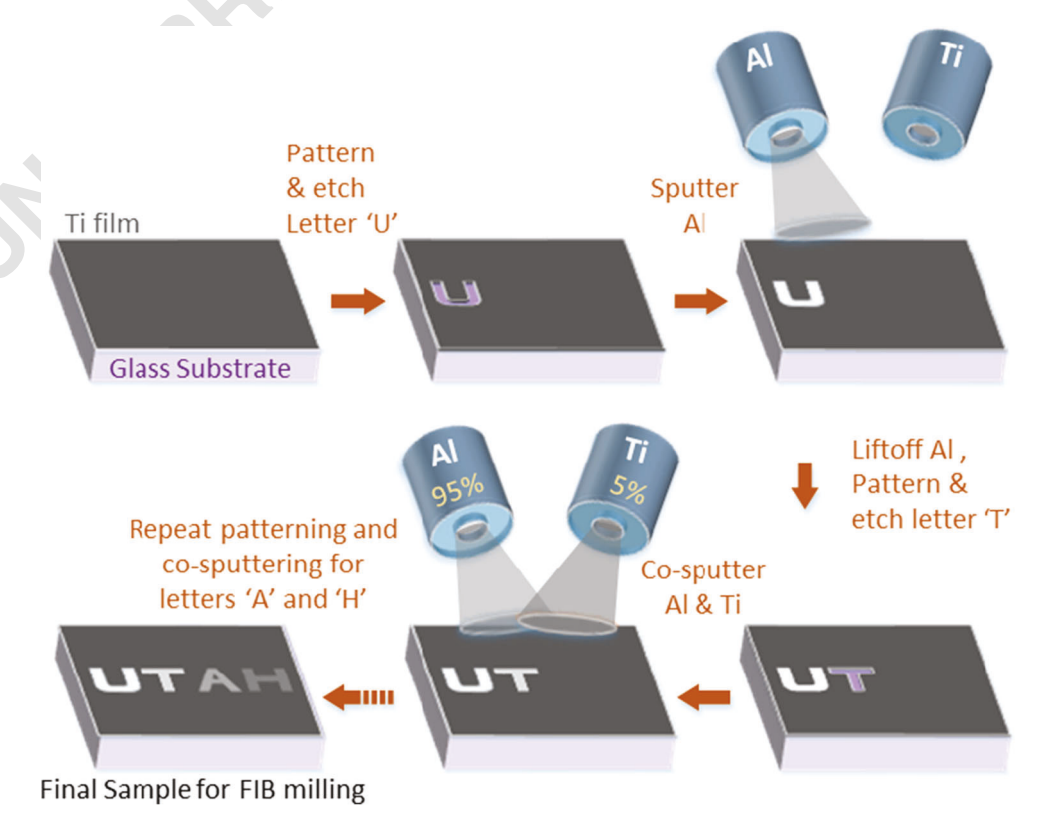
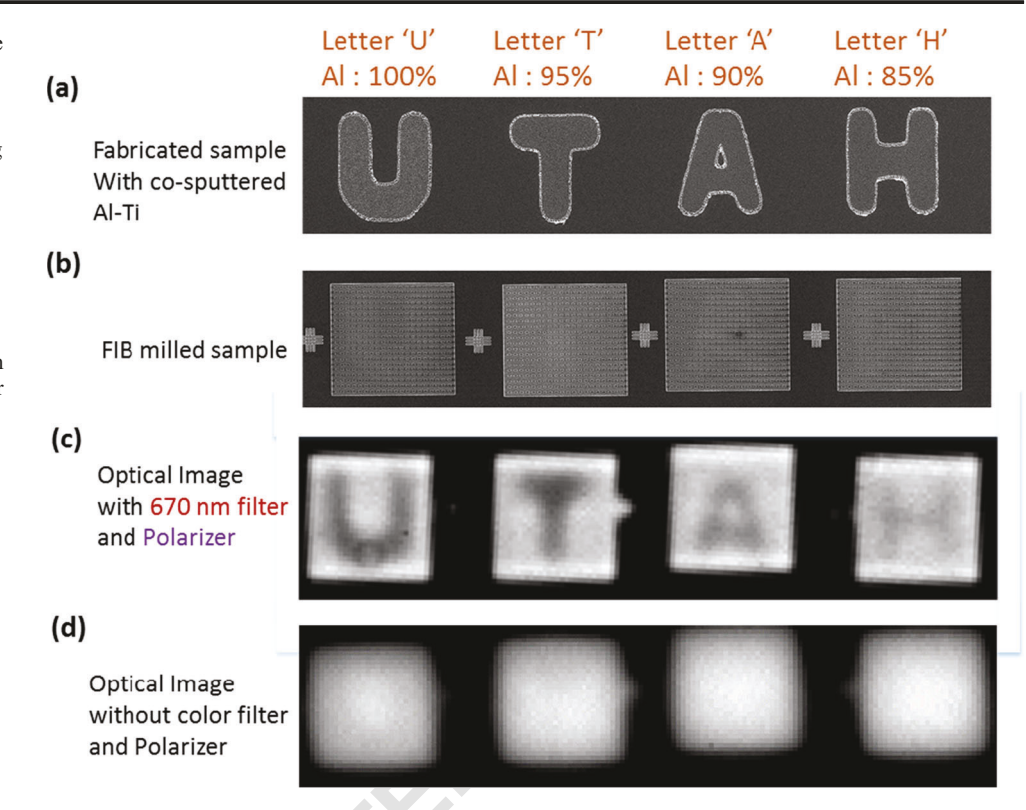




Fig. 5 Measurement results of the grayscale composition-encoded metasurface. a shows the SEM image of final sample obtained after 4 cycles of the co-sputtering process. b SEM image of sample after FIB milling of identical nanorod arrays within areas enclosing the patterned letters. c Optical image upon transmission through grayscale metasurface, measured using a bandpass filter with center wavelength of 670 nm and FWHM of 40 nm and a linear polarizer. The incident light was polarized along the long axis of the nanorods. **d** Control measurement without the optical filter and linear polarizer where no discernable image of encoded letters was observed.



We notice there is a linear relationship between the fraction of Al and the magnitude of transmission within a certain spectral range in both the experimental and simulation results, which implies that transmittance within this range can be manipulated by applying the corresponding fraction of Al in the alloy. We used six alloy compositions in Fig. 2c, which correspond to 100%, 97%, 94%, 90%, 85%, and 80% Al. In principle, any transmittance value from 0.4 to 0.85 can be achieved by co-sputtering the corresponding fractions of Al and Ti (Fig. 2d). The actual dynamic range would have an upper bound of about 88%, which is the estimated (experimental) transmittance if the nanorods were composed entirely of Ti.

With this composition-encoding technique, the phase of transmitted light is independent of amplitude modulation. To illustrate this, we examined the phase profiles of transmitted light through the nanorod arrays with the same size, but different Al:Ti compositions, in FDTD Solutions. In the calculated transmission spectra, resonances are located around the wavelength of 690 nm. Thus, we choose 690 nm as the wavelength for phase comparison. The incident wave in the simulation is polarized along the long axis (x-axis) of the nanorods. The inset of Fig. 2a shows the phase profiles of electric field_x (along the long axis of a rod) for the six different compositions at the wavelength of 670 nm. Across the range of Al varying from 100 to 80%, the phase change of the transmitted light is less than 0.07π . Thus, unlike other

polarization and phase-based spatial light modulation, our approach provides for amplitude modulation while keeping the phase largely unaltered. This approach could be useful towards applications and devices where amplitude-only modulation is desired.

We demonstrated grayscale representation by fabricating nanorod arrays using four different Al:Ti alloy compositions. First, thin films of the four compositions (100%, 95%, 90%, and 85% Al) were deposited with a thickness of 50 nm on four separate glass substrates. Identical 10 × 10 nanorod arrays were fabricated on these four substrates with FIB. Using a microscope, white light passing through a 650-690 nm bandpass filter and a linear polarizer (along the long axis of the nanorods) is incident onto the patterned glass slides. Images observed in the eyepiece were collected by a CCD camera. The images for four separate sets of nanorod are shown in Fig. 3a. Figure 3b shows the linear relationship of the averaged amplitude of each image and the Al percentage, which agrees well with simulation and measurements from Fig. 2.

To further demonstrate grayscale image representation, we designed and fabricated a "U T A H" pattern on a single glass slide. This pattern is fabricated by repeated steps of co-sputtering and photolithography, as sketched in Fig. 4. In this pattern, each letter consists of one Al:Ti composition (for example, U is filled with 100% Al and T is filled with 95% Al). Patterns are surrounded by



100% Ti for light blocking. Thickness for all deposited films is 50 nm. The SEM image for this "U T A H" pattern is shown in Fig. 5a. Then, 20 × 20 nanorod arrays were created for each letter by FIB, with the SEM image shown in Fig. 5b. Using white light, a 650–690 nm bandpass filter, and a linear polarizer with the polarization direction along the nanorod long axis, the complete grayscale image was observed through the microscope (recorded by a CCD camera), as shown in Fig. 5c. This is a raw image observed in the microscope without orientation correction. Letters fade from left to right, as the Al ratio decreases.

To prove that this image can be hidden under white light, we removed the bandpass filter and linear polarizer and obtained the image with the CCD camera, as shown in Fig. 5d. In this image, no clear patterns can be observed. We therefore demonstrated that this metasurface is sensitive to incident light wavelength and polarization direction so that an image (or other encoded information) can be hidden under white light. For both Fig. 5c and d, the intensity of the dark background without patterns was set to zero.

To quantify grayscale contrast and hiding, we have defined two "contrast" parameters based upon comparing the nanorod plasmon responses between compositionencoded rods and pure Ti rods (i.e., the background) in the cases of parallel (long axis) light polarization and unpolarized light. These plots are shown in Fig. S4, using simulated transmission data. We note that these measures vary with wavelength and would be averaged across relevant wavelength ranges depending upon the light source and any polarizers or spectral filters used in the system. These measures could in principle be improved using different geometries. In such case, the image would only be visible under a specific polarization and within a range of frequencies. Moreover, multiple resonant structures within a unit cell could be designed where different images can be encrypted at different wavelength and polarization combinations.

In summary, we demonstrated a new method for image encoding via a subwavelength nanorod array metasurface at optical frequencies. Instead of color printing using varying phases or resonant frequencies, we create an image with multiple gray levels within a narrow wavelength range. In this technique, all nanorods are designed with a common geometry (i.e., common resonant wavelength), and gray levels are encoded through the antenna composition. Although we demonstrated grayscale representation with six levels, in principle, more levels could be achieved by utilizing more points on Fig. 2c, and dynamic range can be increased through further design optimization. Because this technique is sensitive to incident light wavelength and polarization, it could be applied to image hiding/encryption.

Acknowledgments This work was performed in part at the Utah Nanofab, sponsored by the College of Engineering, Office of the Vice President for Research, the Utah Science Technology and Research (USTAR) initiative of the State of Utah, and the NSF MRSEC program. We thank the Surface Analysis and Nano-Scale Imaging Lab at Utah Nanofab for access to ellipsometry and FIB, and help from the supporting staff Brian Baker, Steven Pritchett, Charles Fisher, and Randy C. Polson. The support and resources from the Center for High Performance Computing at the University of Utah are gratefully acknowledged.

Author Contributions The manuscript was written through the contributions of all authors. All authors have given approval to the final version of the manuscript.

Funding Information This work was supported by the NSF MRSEC program at the University of Utah under grant DMR-1121252. Additional support from the ECCS Division of NSF (award 1810096) is acknowledged.

References

- Yu N, Capasso F (2014) Flat optics with designer metasurfaces. Nat 322 Mater 13(2):139–150. https://doi.org/10.1038/nmat3839
- Yu N, Genevet P, Kats MA, Aieta F, Tetienne J-P, Capasso F, Gaburro Z (2011) Light propagation with phase discontinuities: generalized laws of reflection and refraction. Science 334(6054): 333–337. https://doi.org/10.1126/science.1210713
- Verslegers L, Catrysse PB, Yu Z, White JS, Barnard ES, Brongersma ML, Fan S (2009) Planar lenses based on nanoscale slit arrays in a metallic film. Nano Lett 9(1):235–238. https://doi. org/10.1021/nl802830y
- Aieta F, Genevet P, Kats MA, Yu N, Blanchard R, Gaburro Z, Capasso F (2012) Aberration-free ultrathin flat lenses and axicons at telecom wavelengths based on plasmonic metasurfaces. Nano Lett 12(9):4932–4936. https://doi.org/10.1021/nl302516v
- Smith DR, Pendry JB, Wiltshire MCK (2004) Metamaterials and negative refractive index. Science 305(5685):788–792. https://doi. org/10.1126/science.1096796
- Shelby RA, Smith DR, Schultz S (2001) Experimental verification of a negative index of refraction. Science 292(5514):77–79. https:// doi.org/10.1126/science.1058847
- Jiang ZH, Yun S, Lin L, Bossard JA, Werner DH, Mayer TS (2013) Tailoring dispersion for broadband low-loss optical metamaterials using deep-subwavelength inclusions. Sci Rep 3:1571. https://doi. org/10.1038/srep01571
- MacDonald KF, Sámson ZL, Stockman MI, Zheludev NI (2009) Ultrafast active plasmonics. Nat Photonics 3(1):55–58. https://doi. org/10.1038/nphoton.2008.249
- Gao X, Hui Shi J, Shen X, Feng Ma H, Xiang Jiang W, Li L, Jun Cui T (2013) Ultrathin dual-band surface plasmonic polariton waveguide and frequency splitter in microwave frequencies. Appl Phys Lett 102(15):151912. https://doi.org/10.1063/1.4802739
- Ni X, Wong ZJ, Mrejen M, Wang Y, Zhang X (2015) An ultrathin invisibility skin cloak for visible light. Science 349(6254):1310– 1314. https://doi.org/10.1126/science.aac9411
- Chen WT, Yang K-Y, Wang C-M, Huang Y-W, Sun G, Chiang I-D, Liao CY, Hsu W-L, Lin HT, Sun S, Zhou L, Liu AQ, Tsai DP (2014) High-efficiency broadband meta-hologram with polarizationcontrolled dual images. Nano Lett 14(1):225–230. https://doi.org/ 10.1021/nl403811d
- Zheng G, Mühlenbernd H, Kenney M, Li G, Zentgraf T, Zhang S (2015) Metasurface holograms reaching 80% efficiency. Nat Nanotechnol 10(4):308–312. https://doi.org/10.1038/nnano.2015.2



- Huang Y-W, Chen WT, Tsai W-Y, Wu PC, Wang C-M, Sun G, Tsai DP (2015) Aluminum plasmonic multicolor meta-hologram. Nano Lett 15(5):3122–3127. https://doi.org/10.1021/acs.nanolett. 5b00184
- Wan W, Gao J, Yang X (2016) Full-color plasmonic metasurface holograms. ACS Nano 10(12):10671–10680. https://doi.org/10. 1021/acsnano.6b05453
- Kumar K, Duan H, Hegde RS, Koh SCW, Wei JN, Yang JKW (2012) Printing colour at the optical diffraction limit. Nat Nanotechnol 7(9):557–561. https://doi.org/10.1038/nnano.2012.
- Tan SJ, Zhang L, Zhu D, Goh XM, Wang YM, Kumar K, Qiu C-W, Yang JKW (2014) Plasmonic color palettes for photorealistic printing with aluminum nanostructures. Nano Lett 14(7):4023–4029. https://doi.org/10.1021/nl501460x
- Clausen JS, Højlund-Nielsen E, Christiansen AB, Yazdi S, Grajower M, Taha H, Levy U, Kristensen A, Mortensen NA (2014) Plasmonic metasurfaces for coloration of plastic consumer products. Nano Lett 14(8):4499–4504. https://doi.org/10.1021/ nl5014986
- Cheng F, Gao J, Luk TS, Yang X (2015) Structural color printing based on plasmonic metasurfaces of perfect light absorption. Sci Rep 5:11045. https://doi.org/10.1038/srep11045
- Franklin D, Chen Y, Vazquez-Guardado A, Modak S, Boroumand J, Xu D, Wu S-T, Chanda D (2015) Polarization-independent actively tunable colour generation on imprinted plasmonic surfaces. Nat Commun 6:7337. https://doi.org/10.1038/ncomms8337
- Kristensen A, Yang JKW, Bozhevolnyi SI, Link S, Nordlander P, Halas NJ, Mortensen NA (2017) Plasmonic colour generation. Nat Rev Mater 2:16088. https://doi.org/10.1038/natrevmats.2016.88
- Duan X, Kamin S, Liu N (2017) Dynamic plasmonic colour display. Nat Commun 8:14606. https://doi.org/10.1038/ ncomms14606
- Shu F-Z, Yu F-F, Peng R-W, Zhu Y-Y, Xiong B, Fan R-H, Wang Z-H, Liu Y, Wang M (2018) Dynamic plasmonic color generation

- based on phase transition of vanadium dioxide. Adv Opt Mater 6(7). https://doi.org/10.1002/adom.201700939
- Duan X, Liu N (2018) Scanning plasmonic color display. ACS Nano 12(8):8817–8823. https://doi.org/10.1021/acsnano.8b05467
- Franklin D, Modak S, Vázquez-Guardado A, Safaei A, Chanda D (2018) Covert infrared image encoding through imprinted plasmonic cavities. Light: Science & Applications 7(1):93. https://doi.org/ 10.1038/s41377-018-0095-9
- Yue F, Zhang C, Zang X-F, Wen D, Gerardot BD, Zhang S, Chen X (2018) High-resolution greyscale image hidden in a laser beam. Light Sci Appl 7(1):17129. https://doi.org/10.1038/lsa.2017.129
- Farmahini-Farahani M, Cheng J, Mosallaei H (2013) Metasurfaces nanoantennas for light processing. J Opt Soc Am B 30(9):2365– 2370. https://doi.org/10.1364/JOSAB.30.002365
- Liu L, Zhang X, Kenney M, Su X, Xu N, Ouyang C, Shi Y, Han J, Zhang W, Zhang S (2014) Broadband metasurfaces with simultaneous control of phase and amplitude. Adv Mater 26(29):5031–5036. https://doi.org/10.1002/adma.201401484
- Novotny L (2007) Effective wavelength scaling for optical antennas. Phys Rev Lett 98(26):266802. https://doi.org/10.1103/ PhysRevLett.98.266802
- West PR, Ishii S, Naik GV, Emani NK, Shalaev VM, Boltasseva A (2010) Searching for better plasmonic materials. Laser Photonics Rev 4(6):795–808. https://doi.org/10.1002/lpor.200900055
- Knight MW, Liu L, Wang Y, Brown L, Mukherjee S, King NS, Everitt HO, Nordlander P, Halas NJ (2012) Aluminum plasmonic nanoantennas. Nano Lett 12(11):6000–6004. https://doi.org/10. 1021/nl303517v
- 31. Blaber MG, Arnold MD, Ford MJ (2010) A review of the optical properties of alloys and intermetallics for plasmonics. J Phys Condens Matter 22(14):143201. https://doi.org/10.1088/0953-8984/22/14/143201

Publisher's Note Springer Nature remains neutral with regard to jurisdictional claims in published maps and institutional affiliations.

